Results in Physics 47 (2023) 106380

Contents lists available at ScienceDirect

Results in Physics

journal homepage: www.elsevier.com/locate/rinp

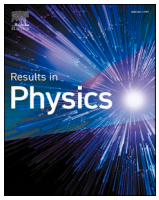

Raman spectroscopy of lithium niobate ($LiNbO_3$) – Sample temperature and laser spot size effects

A.R. Zanatta

Instituto de Física de São Carlos, USP, São Carlos 13560-970 – SP, Brazil

ARTICLE INFO

Keywords:
Lithium niobate ($LiNbO_3$)
Raman scattering
Phonon coupling
Temperature-dependence

ABSTRACT

The Raman spectrum of lithium niobate ($LiNbO_3$) was investigated in the 83–823 K temperature range and as a function of different laser spot sizes. The measurements considered a Z-cut (congruent, undoped) $LiNbO_3$ crystal, HeNe laser excitation (632.8 nm photons), and the $z(x,xy)\bar{z}$ geometry. The main $LiNbO_3$-related phonon modes were identified and analyzed in terms of their peak position (ω) and linewidth (γ), according to which it was possible to identify the contributions originating from anharmonic phonon-coupling and thermal lattice-expansion processes. The analyses of the temperature-dependent $\omega(T)$ and $\gamma(T)$ data took into account the 3- and 4-phonon model and the experimental Grüneisen and linear thermal expansion coefficients – as available from literature. Among all phonon modes of $LiNbO_3$, the A1(TO4) mode presented a peculiar behavior (at room temperature) that depends on the laser spot size during the Raman measurements. The development of this forbidden mode has been associated with the congruent-photorefractive nature of $LiNbO_3$ as well as with small variations in the geometry of polarization (as a result of changes in the laser spot size).

Introduction

One of the first scientific reports on lithium niobate ($LiNbO_3$) dates from 1949, when niobium was referred to as columbium (or $LiCbO_3$), and it was about its ferroelectric properties. [1] The work was followed by several studies – most of them carried out at the Bell Laboratories [2] – demonstrating the nonlinear optical behavior of $LiNbO_3$, [3] as well as by indicating the best ways to produce good quality crystals. [4] $LiNbO_3$ is a manmade material that, because of its (trigonal) crystal structure and (adjustable) atom composition, presents remarkable pyroelectric, [5] photoelastic, [6] photorefractive, [7] photovoltaic, [8] piezoelectric, [9] and electrooptic [10] characteristics. Within the various $LiNbO_3$-related applications one can mention those in the fields of photonics, [11] wavelength (or surface acoustic wave) filters, [12,13] optical waveguides (modulators), [14,15] optical frequency converters (oscillators) [16,17] and, more recently, those involving the development of temperature-sensors [18] and chip-based devices [19] – just to mention a few of them. Since the successful device application of $LiNbO_3$ crystals is determined by their main properties, it is essential to know the atom composition and structure of $LiNbO_3$ in detail – ideally by varying its measurement conditions over extensive-useful ranges. Usually, $LiNbO_3$ is prepared by the Czochralski technique and, depending on the growth conditions, the crystals can be stoichiometric, near-stoichiometric (or off-congruent), or non-stoichiometric (or congruent). Albeit congruent $LiNbO_3$ crystals (*i.e.*, $[Li_2O] \sim 48.5 \pm 0.5$ mol%) are known to contain large concentrations of niobium anti-sites (Nb_{Li}^{5+}) and/or lithium vacancies (V_{Li}^{1-}) [20] they respond for most of the current technological applications. [21] Furthermore, commercial $LiNbO_3$ is available in different crystallographic orientations, in which case the cutting–polishing of the crystal slices can influence its final properties. Some of these compositional and structural characteristics of $LiNbO_3$ can be probed by Raman scattering spectroscopy that, additionally, is able to provide valuable lattice-dynamic information (such as those involving the anharmonic behavior of phonons) [22,23].

Motivated by the above aspects, this work presents a detailed Raman investigation of a crystalline (Z-cut) congruent $LiNbO_3$ sample. The study is divided in two parts: the first one regarding the identification of the main phonon modes of $LiNbO_3$ and the influence of the external temperature on their characteristic Raman signal frequency and linewidth. This part also includes the theoretical analyses of the experimental data according to phonon-coupling and thermal expansion models. In the second part, the dependence of the signal intensity of the A1(TO4) phonon mode with the laser spot size is analyzed in detail.

Experimental

A commercial $LiNbO_3$ single crystal (2-side optical-grade polished, Z-cut, congruent, ferroelectric, undoped, 500 μm thick) [24] was considered in the study. The Z-cut character of the crystal was confirmed by Raman polarized measurements, demonstrating that the main surface of the sample is perpendicular to the c crystallographic axis (see Fig. S1 -Supplementary Material).[22,23] The crystal composition was verified by

https://doi.org/10.1016/j.rinp.2023.106380
Received 10 February 2023; Received in revised form 10 March 2023; Accepted 18 March 2023
Available online 21 March 2023

combining either the linewidths of certain Raman modes or the optical absorption edge of $LiNbO_3$ with proper calibration curves. [25,26] Following this procedure, the relative amount of Li_2O in $LiNbO_3$ was found to be $\sim 48.5 \pm 0.3$ mol% (see Figs. S2 and S3 -Supplementary Material). [27] The Raman measurements were carried out in a microprobe setup (*Renishaw* RM2000) by exciting the sample surface with 632.8 nm photons under the $z(x,xy)\bar{z}$ backscattering geometry (see Fig. S1 -Supplementary Material). The Raman spectra in the 83–823 K temperature range (in steps of either 25 or 50 K) were obtained via a computer-controlled temperature-stage (*Linkam* THMS600). In this case, a 50x long-working distance objective (NA = 0.55, laser power density $\sim$ 0.4 mW μm^{-2}) was employed, and a dwell time of 3 min was adopted to guarantee that thermal equilibrium has been reached before each spectrum scan. Additional Raman measurements, at room conditions, included various laser powers and spot sizes – as obtained by means of different objective lenses (20x, 50x and 100x) in combination with a laser beam expander (see Fig. S4 -Supplementary Material). In all cases, a typical $\pm$ 2 cm^{-1} uncertainty was ascribed to the Raman data and, over the length of hours, most of the spectra have been checked to confirm their reproducibility.

Results & discussion

A. Sample temperature effects.

The Raman spectra of the $LiNbO_3$ crystal at some selected temperatures are presented in Fig. 1. At first sight, it is evident the red-shift and signal broadening of the Raman lines as the temperature advances. The proper identification of these lines along with their deconvolution into, for example, Lorentzian curves help to understand this temperature-induced effect as well as allow to obtain some important properties of the $LiNbO_3$ crystal.

Under C3v symmetry, Group Theory predicts that the irreducible representations of the $LiNbO_3$-related phonons at the center of the Brillouin zone can be described by 5A1 + 5A2 + 10E. As a result: [22,23] (a) the A2 modes are silent; (b) excluding two acoustic phonon modes (one E and one A1), all the others are optical – both Raman and infrared active; (c) usually, dipole moments along the X (or Y) and Z axis are associated, respectively, with E and A1 phonon modes; and (d) owing to its ionic nature, the E and A1 modes of $LiNbO_3$ present transverse and longitudinal components. Furthermore, and of special importance to this work: (e) the incidence of all phonon modes predicted by Group Theory takes place exclusively in stoichiometric $LiNbO_3$; (f) under backscattering geometry, only the transverse (TO) and longitudinal (LO) optical modes with E and A1 symmetries will be apparent in the Raman spectrum of $LiNbO_3$; and (g) the development of unexpected phonon modes (*i.e.*, the advent of modes different of those anticipated by Group Theory or symmetry conditions) originates because of instrumental (polarization misalignment) and/or sample's (composition variations, presence of defects, disorder, etc.) problems. Based on these facts, the only Raman features supposed to occur in the $LiNbO_3$ crystal (Z-cut and $z(x,xy)\bar{z}$ geometry) are those related to the E and A1 symmetries, respectively associated with the TO and LO phonon modes. Fig. 2 shows the Raman spectrum of $LiNbO_3$ along with the identification of its main phonon modes:[23] E(TO1) at $\sim$ 152 cm^{-1}, E(TO2) at $\sim$ 187 cm^{-1}, E(TO3) at $\sim$ 236 cm^{-1}, E(TO4) at $\sim$ 264 cm^{-1}, A1(LO1) at $\sim$ 278 cm^{-1}, E(TO5) at $\sim$ 323 cm^{-1}, A1(LO2) at $\sim$ 336 cm^{-1}, E(TO6) at $\sim$ 369 cm^{-1}, A1(LO3) at $\sim$ 421 cm^{-1}, E(TO7) at $\sim$ 433 cm^{-1}, E(TO8) at $\sim$ 580 cm^{-1}, A1(TO4) at $\sim$ 622 cm^{-1}, E(TO9) at $\sim$ 739 cm^{-1}, A1(LO4) at $\sim$ 871 cm^{-1}, and E (LO9) at $\sim$ 896 cm^{-1}.

Except for two forbidden modes – A1(TO4) and E(LO9) – and one unidentified mode (at $\sim$ 670 cm^{-1}), the experimental results agree with Group Theory. Whereas the appearance of these unwanted Raman signals can occur due to a combination of sample – experimental conditions, the A1(TO4) mode (at $\sim$ 622 cm^{-1}) deserves special attention and it will be considered in the next section.

In order to explore the phonon dynamics of the $LiNbO_3$ crystal some of the most prominent E(TO) and A1(LO) Raman modes have their phonon frequencies and linewidths analyzed in detail. The results of this investigation are presented in Fig. 3 and Fig. 4.

In a temperature-dependent Raman experiment, the factors that most influence the Raman signal peak frequency (ω) and linewidth (γ) are due to anharmonic phonon–phonon interactions and/or resulting from thermal expansion effects. [28] Accordingly, the $\omega(T)$ and $\gamma(T)$ analyses provide relevant physical–chemical information as well as details regarding the influence of impurities or defects. [23] The theory behind the T-dependent phonon behavior of solids can be found in many works [29] and, usually, it is based on the decay of one phonon into two (3-phonon 3p process) and three phonons (4-phonon 4p process) according to the Bose-Einstein phonon population factor. As a result, at constant pressure, the T-induced variation of the Raman signal peak frequency due to phonon coupling (ω_{PC}) is:

$$\omega_{PC}(T) = \omega_0 + \Omega_{3p}\left[1 + \frac{2}{\exp(\hbar\omega_0/2k_BT) - 1}\right] + \Omega_{4p}\left[1 + \frac{3}{\exp(\hbar\omega_0/3k_BT) - 1} + \frac{3}{[\exp(\hbar\omega_0/3k_BT) - 1]^2}\right], \quad (1)$$

where ω_0 is the Raman signal peak frequency at T $\sim$ 0 K, Ω_{3p} and Ω_{4p} are phonon anharmonic constants, and $\hbar$ and k_B stand for the reduced Planck and Boltzmann constants.

Regarding the T-induced thermal expansion (or quasiharmonic) contribution (ω_{TE}), it can be expressed as:

$$\omega_{TE}(T) = \omega_0\left[\exp\left(-3\delta\int_0^T \alpha(T)dT\right) - 1\right], \quad (2)$$

where δ is the isotherm mode Grüneisen parameter and $\alpha(T)$ is the linear thermal expansion coefficient. Altogether, the T-dependent Raman signal peak frequency behavior can be described by:

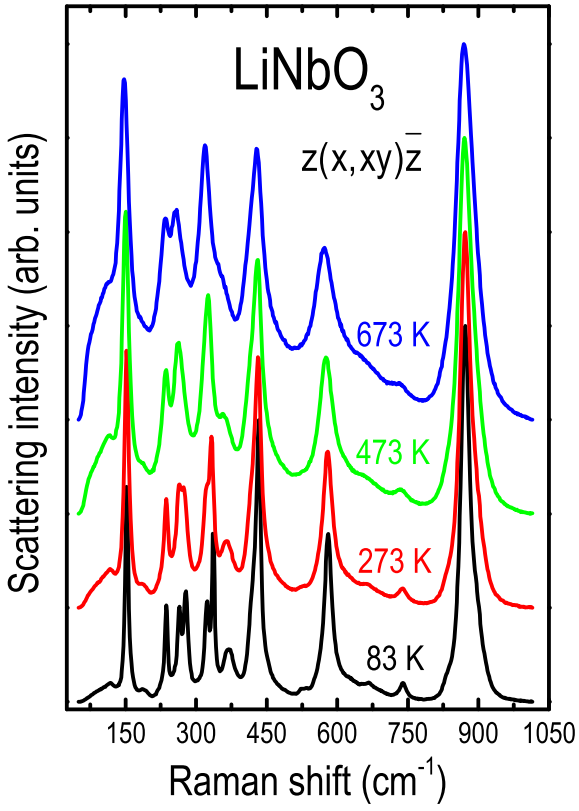

Fig. 1. Raman scattering spectra (632.8 nm photon excitation, $z(x,xy)\bar{z}$ geometry) of a $LiNbO_3$ single crystal (Z-cut) at 83, 273, 473, and 673 K. The spectra were normalized and vertically shifted for comparison reasons.

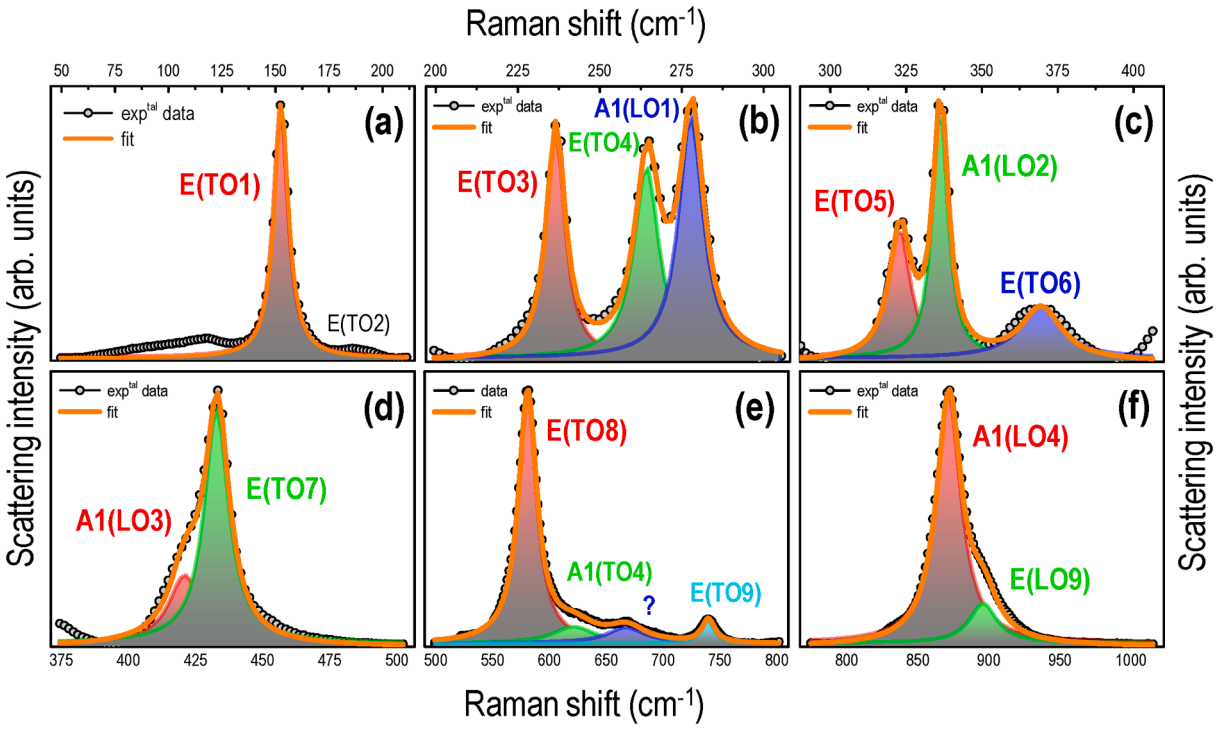

Fig. 2. Raman spectra ($z(x,xy)\bar{z}$ geometry) of a Z-cut $LiNbO_3$ crystal, at 83 K. For clarity reasons the ~ 50–1000 cm^{-1} spectrum was separated in parts, normalized, and the main Raman phonon modes were indicated by their corresponding Lorentzian curve fittings. (a) E(TO1) and E(TO2); (b) E(TO3), E(TO4) and A1(LO1); (c) E(TO5), A1(LO2) and E(TO6); (d) A1(LO3) and E(TO7); (e) E(TO8), A1(TO4), unknown mode and E(TO9); (f) A1(LO4) and E(LO9).

$$\omega(T) = \omega_{PC}(T) + \omega_{TE}(T) \tag{3}$$

A similar reasoning – involving the phonon (anharmonic) relaxation processes – applies to the T-induced variation of the Raman signal linewidth (γ), or FWHM height of the Raman signal, such that:

$$\gamma(T) = \gamma_0 + \Gamma_{3p}\left[1 + \frac{2}{\exp(\hbar\omega_0/2k_BT) - 1}\right] + \Gamma_{4p}\left[1 + \frac{3}{\exp(\hbar\omega_0/3k_BT) - 1} + \frac{3}{[\exp(\hbar\omega_0/3k_BT) - 1]^2}\right], \tag{4}$$

where – in addition to $\hbar$ and k_B already introduced in Eq. (1) – γ_0 is the Raman signal linewidth at T ~ 0 K, and Γ_{3p} and Γ_{4p} are anharmonic constants relating 3- and 4-phonon processes.

Fig. 3 shows the Raman signal peak frequency and linewidth of some E(TO) modes of $LiNbO_3$ as obtained by Lorentzian curve fitting of the experimental spectra in the 83–823 K temperature range. The figure also shows the $\omega(T) = \omega_{PC}(T) + \omega_{TE}(T)$ and $\gamma(T)$ theoretical results as provided by the 3- and 4-phonon approach – see Eqs. (1) to (4). In this case, the fitting of the experimental Raman(T) data with the theoretical expressions took into account the corresponding Grüneisen parameters and the linear thermal expansion coefficients, as available from literature. [30,31] The main results of this fitting procedure are presented in Table 1.

The very same procedure has been applied to analyze the Raman T-dependence of some A1(LO) phonon modes, and the results are shown in Fig. 4 and Table 1.

Considering an experimental uncertainty of approx. ± 2 cm^{-1} (spectrometer resolution ~ 1.5 cm^{-1} + data dispersion ~ 0.5 cm^{-1}), the results of Figs. 3 and 4 indicate a rather good agreement between theory and experiment – in the 83–823 K temperature range – suggesting the suitability of the model to describe the phonon behavior of Z-cut $LiNbO_3$. In fact, without ignoring the influence of defects (and/or disorder), the present T-dependent Raman analyses clearly show the distinctive contributions due to anharmonic phonon-coupling processes and simple lattice expansion in determining the whole $\omega(T)$ and $\gamma(T)$ experimental behavior. Further improvements to this study should consider the use of $LiNbO_3$ of different compositions and crystal orientations, as well as a wider temperature range.

B. Laser spot size effects.

At room temperature, while performing the Raman experiments with different geometry polarizations, a curious aspect came out by varying the microscope objective lenses. Regardless of the sample region, the A1 (TO4) phonon mode exhibited a Raman signal intensity that scales with the laser spot size. The effect is very reproducible and, even after different laser exposure times and Raman signal normalization, the whole spectrum is exactly the same – except for the intensity of the A1 (TO4) mode. This effect can be seen in Fig. 5(a) that shows the room temperature Raman spectra of $LiNbO_3$ at increasing laser spot sizes. The spectra were obtained with a 20x objective lens (NA = 0.40 and fixed 3.2 mW laser power) and the laser spot sizes were computer-controlled by means of a beam expander (see Fig. S4 -Supplementary Material).

The spectra of Fig. 5(a) were deconvoluted according to the individual phonon contributions [Fig. 5(b), 5(c), and 5(d)], and their Raman signal integrated areas are displayed in Fig. 5(e). Based on the results, it is clear the development of the A1(TO4) Raman mode as the laser spot size increases from 16 to 6500 μm^2.

Despite the very low optical absorption of 632.8 nm photons (see Ref [27] and Fig. S3 -Supplementary Material), and the absence of any obvious temperature-induced effect (like Raman signal line shifting and/or broadening), the results of Fig. 5 may possibly be influenced by the laser power density. In this case, the Raman signal intensity of the A1 (TO4) phonons was determined essentially by the total number of the incoming photons. The idea applies to any phonon mode in the sense that, ideally: (1) under fixed laser spot sizes, the Raman signal intensity increases with the laser power, and (2) at fixed laser powers, the Raman signal intensity remains practically constant (or decreases due to light reflection losses) with increasing spot sizes. In order to test this hypothesis additional measurements were performed, which included the

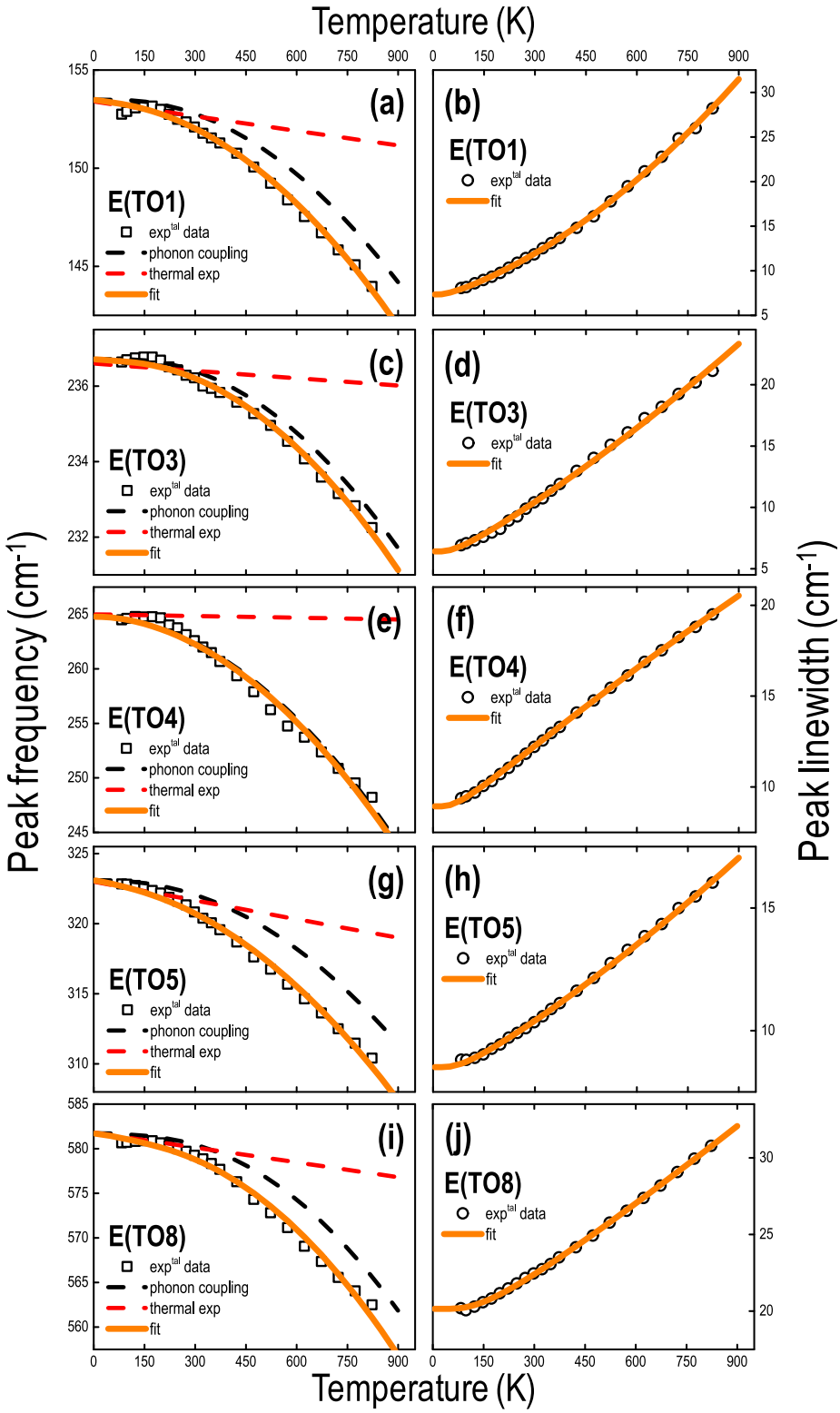

Fig. 3. Raman signal peak frequency (ω) and linewidth (γ) of $LiNbO_3$ (Z-cut, $z(x,xy)\bar{z}$ geometry) as a function of temperature. The figures show the experimental data (as obtained by Lorentzian curve fittings), along with the theoretical $\omega(T) = \omega_{PC}(T) + \omega_{TE}(T)$ and $\gamma(T)$ results of the E(TO) phonon modes: (a)+(b) E(TO1); (c)+(d) E(TO3); (e)+(f) E(TO4); (g)+(h) E(TO5); and (i)+(j) E(TO8).

Table 1
Physical quantities obtained by fitting the experimental $\omega(T)$ and $\gamma(T)$ data of $LiNbO_3$ (Z-cut, $z(x,xy)\bar{z}$ geometry), according to the theoretical model involving 3- and 4-phonon processes – see Eqs. (1) to (4). In all phonon modes, a linear thermal expansion coefficient $\alpha = 3.8x10^{-6}$ K^{-1} has been adopted. [31].

Mode	ω_0 (cm^{-1})	Ω_{3p} (cm^{-1})	Ω_{4p} (cm^{-1})	$\delta^{\#}$	γ_0 (cm^{-1})	Γ_{3p} (cm^{-1})	Γ_{4p} (cm^{-1})
E(TO1)	153.0	0.111	−0.024	1.44	6.6	0.687	0.030
E(TO3)	236.6	0.150	−0.034	0.24	5.7	1.394	0.019
E(TO4)	264.5	−0.077	−0.133	0.17	7.4	1.550	−0.010
E(TO5)	322.0	0.237	−0.131	1.22	7.5	0.992	0.017
E(TO8)	581.5	2.648	−0.929	0.84	20.0	3.294	0.025
A1(LO1)	278.0	−0.473	−0.127	2.20	7.7	1.549	−0.005
A1(LO2)	336.5	−1.542	−0.126	0.74	5.2	1.868	0.096
A1(LO4)	871.2	2.158	−0.879	0.25	21.5	10.545	−0.408

$^{\#}$ Experimental Grüneisen parameter of $LiNbO_3$ crystal, [30] except for the A1(LO4) mode that was assumed to be 0.25.

use of different laser powers and the analysis of other phonon modes as well. The results of these investigations are summarized in Fig. 6.

Fig. 6(a) and 6(b) show the Raman signal intensity of the most prominent phonon modes of the $LiNbO_3$ crystal – A1(LO4), E(TO1), E(TO7) and E(TO8) – and the forbidden A1(TO4) mode as a function of the laser power and laser spot size. The measurements were carried out at room conditions (20x objective lens and $z(x,xy)\bar{z}$ geometry) by imposing a fixed spot size of 16 μm^2 [Fig. 6(a)] and a fixed laser power of 3.2 mW [Fig. 6(b)].

As expected, the Raman intensity of all modes increased (*decreased*) with the laser power (*spot size*) – in a clear indication of the average number of photons participating in the Raman scattering process. If, instead of the absolute Raman signal intensity I_{mode}, one considers the Raman signal intensity ratio between the A1(TO4) and E(TO8) modes (*i.e.*, $I_{Ratio} = \frac{I_{A1(TO4)}}{I_{E(TO8)}+I_{A1(TO4)}}$) the results indicate: a practically constant I_{Ratio} as the laser power advances [Fig. 6(c)], in contrast to the growing I_{Ratio} as the laser spot size is increased [Fig. 6(d)]. In fact, the use of I_{Ratio} illustrates the A1(TO4) phonon behavior more clearly and it is exempt from problems involving the absolute Raman signal intensity and/or the advent of any spectrum background.

Finally, representing I_{Ratio} as a function of the laser power density (*i.e.*, the laser power divided by the laser spot area) allows to investigate the development of the A1(TO4) mode in terms of the average number of photons reaching the $LiNbO_3$ surface. These results are presented in Fig. 6(e) that shows the I_{Ratio} ratios of the rough Raman signal intensities (open symbols) and corresponding Raman integrated areas (filled symbols), as obtained from different objective lenses and laser beam expander conditions. According to Fig. 6(e), as the laser power density increases from ~ 1 to 10^3 μW μm^{-2} (which is equivalent to shrink the laser spot size from approx. 10^4 to 1 μm^2) the I_{Ratio} ratios: (i) remain practically constant when probed by a 100x objective lens (squares in the figure), (ii) experience some reduction with the 50x lens (triangles), and (iii) clearly decrease when a 20x lens is used (stars). Considering the

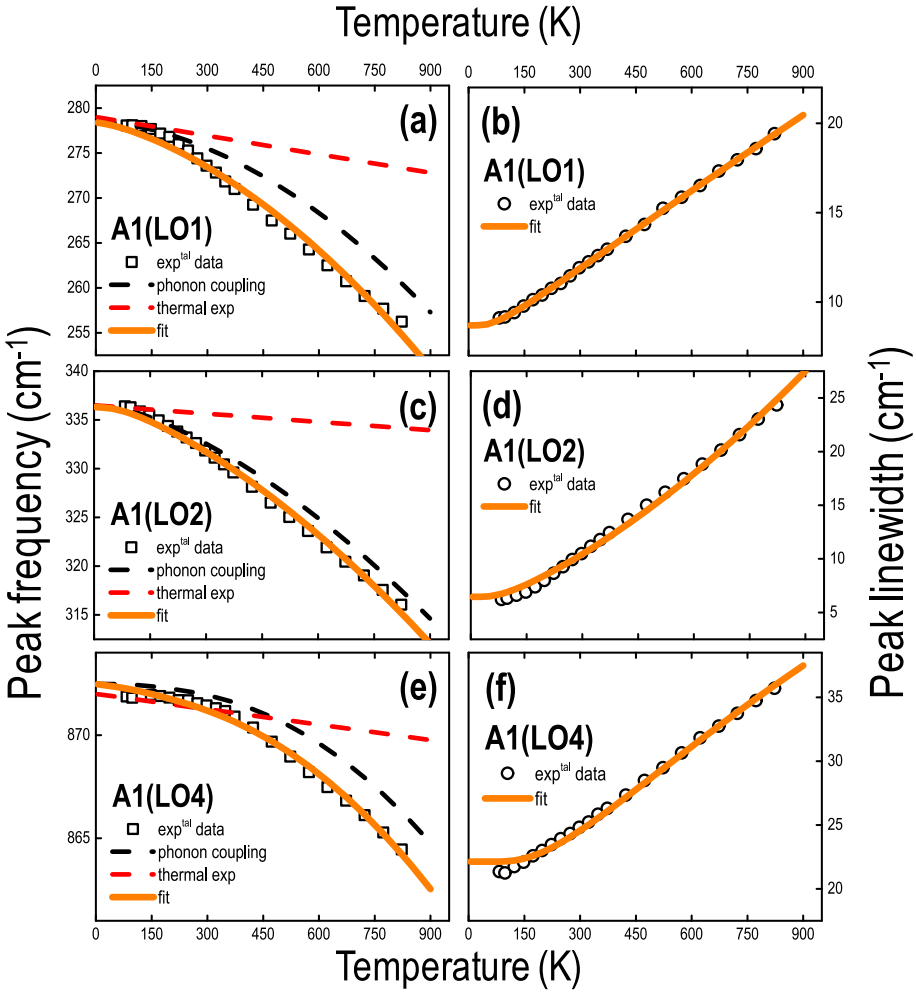

Fig. 4. Raman signal peak frequency (ω) and linewidth (γ) of $LiNbO_3$ (Z-cut, $z(x,xy)\bar{z}$ geometry) as a function of temperature. The figures show the experimental data (as obtained by Lorentzian curve fittings), along with the theoretical $\omega(T) = \omega_{PC}(T) + \omega_{TE}(T)$ and $\gamma(T)$ results regarding the A1(LO) phonon modes: (a)+(b) A1(LO1); (c)+(d) A1(LO2); and (e)+(f) A1(LO4).

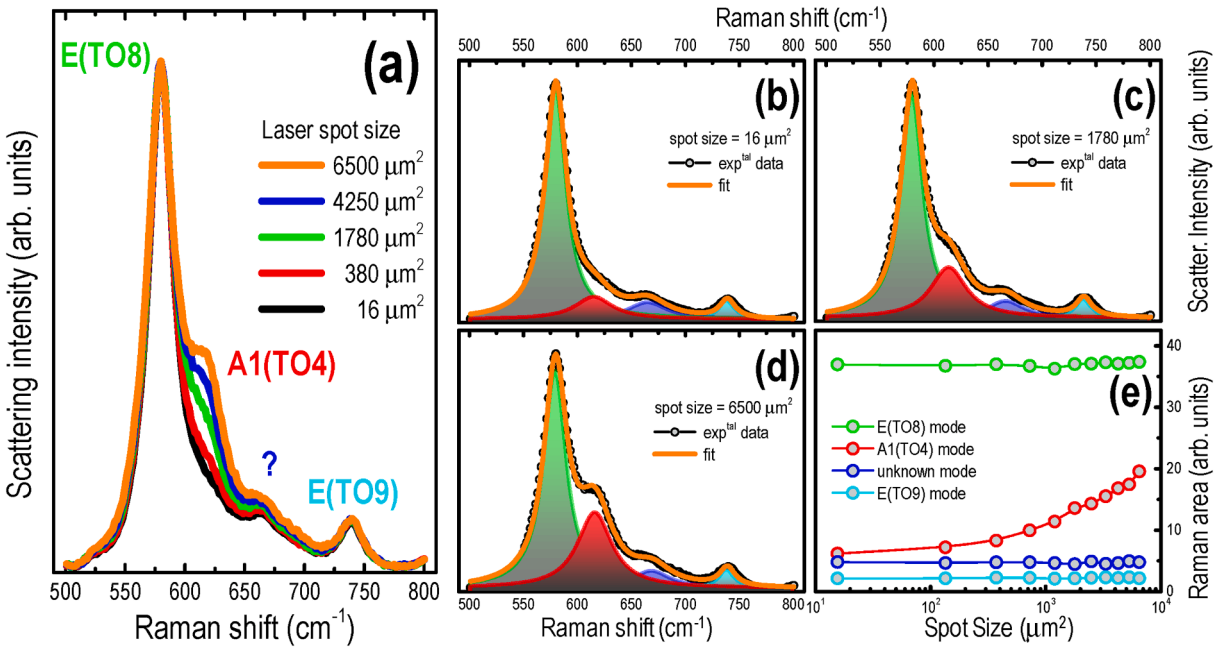

Fig. 5. (a) Room temperature Raman spectra of a Z-cut $LiNbO_3$ crystal ($z(x,xy)\bar{z}$ geometry), in the 500–800 cm^{-1} range, as obtained by increasing the laser spot size from 16 to 6500 μm^2. The spectra – acquired with a 20x objective lens and fixed 3.2 mW laser power – were normalized for comparison purposes. (b)+(c)+(d) Examples of Raman spectra achieved under different laser spot sizes and their deconvolution into individual phonon-related Lorentzian curves. (e) Raman signal integrated areas (after Lorentzian curve fitting) of the E(TO8), A1(TO4), unknown, and E(TO9) phonon modes as a function of the laser spot sizes.

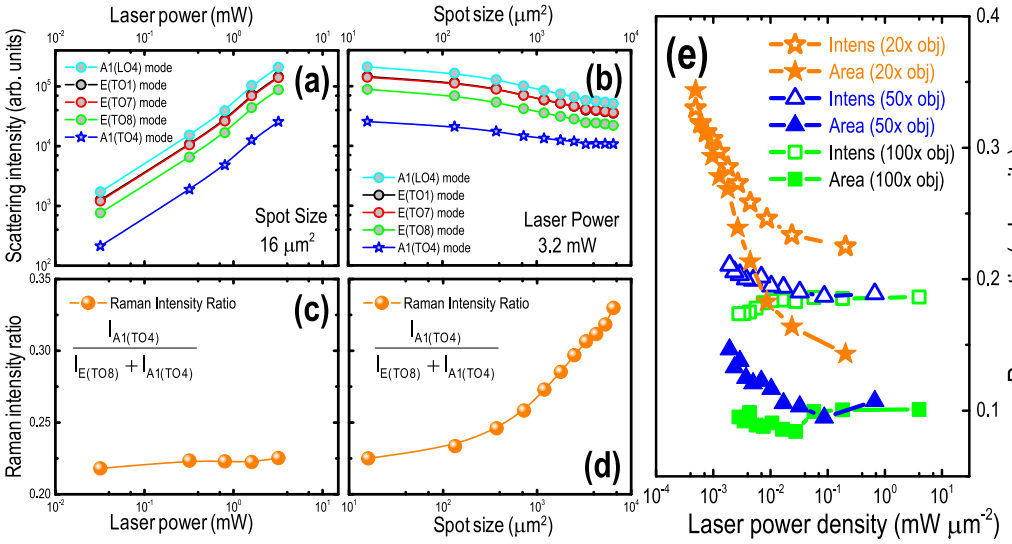

Fig. 6. Room temperature Raman results of a Z-cut $LiNbO_3$ crystal by using a 20x objective lens and $z(x,xy)\bar{z}$ geometry. Raman signal intensity of the A1(LO4), E(TO1), E(TO7), E(TO8), and A1(TO4) phonon modes as a function of: (a) the laser power (fixed spot size of 16 μm^2), and (b) the laser spot size (fixed laser power of 3.2 mW). Raman signal intensity ratio relating the A1 (TO4) and E(TO8) modes as a function of: (c) the laser power (fixed spot size of 16 μm^2), and (d) the laser spot size (fixed laser power of 3.2 mW). (e) Raman signal (intensity and area) ratios – as obtained with 20x, 50x, and 100x objective lenses – as a function of the laser power density (*i.e.*, laser power divided by the laser spot area).

precise laser spot sizes – in the ~ 16–6500 μm^2 (20x lens), ~3.5–1200 μm^2 (50x lens), and ~ 0.2–270 μm^2 (100x lens) ranges – the experimental results suggest that the A1(TO4)-related Raman signal is apparent only at laser spot sizes larger than ~ 300 μm^2, corresponding to laser power densities below approx. 30 $\mu W\ \mu m^{-2}$ [Fig. 6(e)].

Taking into account that the A1(TO4) mode is not expected to occur in Z-cut $LiNbO_3$ under the $z(x,xy)\bar{z}$ geometry, its appearance can be ascribed to the photorefractive nature [32] of $LiNbO_3$ and/or to the presence of defects (either due to composition deviations [33] or resulting from ion bombardment processes [34,35]). As a matter of fact, since the A1(TO4) mode corresponds to symmetric vibrations of the oxygen octahedra O6, its relative signal intensity has been successfully considered as a good measure of the photorefractive effect in $LiNbO_3$ single crystals.[32,33] In addition to the photorefractive effect, the development of the A1(TO4) mode should also be influenced by small changes in the geometry of measurement. It happens because, under the present conditions (*i.e.*, backscattering and by means of short focal length lens) the parallelism of the incoming – scattered laser beams can be altered giving rise to unexpected polarization geometries. [36].

At this point, it is clear that the (forbidden) A1(TO4) phonons arise owing to the congruent-photorefractive behavior of $LiNbO_3$ and/or because of polarization variations during the Raman measurements. In the former case, the effect is susceptible to (compositional – structural) defects present in the $LiNbO_3$ crystal. In the latter, extra – unknown polarization geometries reinforce the development of the A1(TO4) mode as a result of different laser spot sizes. Neither the exact nature of these defects (Li vacancies and/or Nb anti-sites) nor the origin of what seems to be a minimum laser spot size (~300 μm^2) can be precisely explained

by means of the current experimental data. However, given the importance of Z-cut $LiNbO_3$ crystals in technological applications, allied to their strong polar character, [37] future work on this subject may involve the use of $LiNbO_3$ crystals of different compositions as well as the information provided by complementary techniques (like x-ray photoelectron spectroscopy and atomic force microscopy, for example).

Concluding remarks

The Raman spectrum of $LiNbO_3$ was achieved in the 83–823 K temperature range. The measurements considered a (congruent, undoped) Z-cut $LiNbO_3$ crystal, 632.8 nm photon excitation, and the $z(x,xy)\bar{z}$ polarization geometry. After proper identification of the main phonon modes, they were analyzed in terms of the corresponding Raman signal peak frequency (ω) and linewidth (γ) – as obtained from Lorentzian curve fittings. The experimental temperature-dependent $\omega(T)$ and $\gamma(T)$ results are consistent with the 3- and 4-phonon model, according to which it was possible to separate the anharmonic phonon-coupling processes from the lattice thermal expansion contributions. Given the congruent nature of the $LiNbO_3$ crystal, the Raman spectra showed the presence of the forbidden A1(TO4) phonon mode. A thorough inspection of this mode indicated a close connection between its signal intensity (or integrated area) and the laser spot size during the measurements. Accordingly, the development of the A1(TO4) mode has been associated with the inherent congruent-photorefractive character of the $LiNbO_3$ crystal as well as with eventual changes in the polarization geometry of measurement. Further information of the above described (temperature-induced and spot size) effects can be achieved by investigating $LiNbO_3$ of different crystal composition – orientation, wider temperature ranges, as well as by exploring the properties of $LiNbO_3$ with (surface-sensitive) supplementary techniques.

Declaration of Competing Interest

The authors declare that they have no known competing financial interests or personal relationships that could have appeared to influence the work reported in this paper.

Data availability

Data available in article supplementary material or on request.

Acknowledgments

The author is indebted to Professor Máximo Siu Li (USP) and Professor Tomaz Catunda (USP) for critical reading the manuscript.

This work was financially supported by the Brazilian agencies CNPq (Grant 304569/2021-6) and FAPESP.

Appendix A. Supplementary data

Supplementary data to this article can be found online at https://doi.org/10.1016/j.rinp.2023.106380.

References

[1] Matthias BT, Remeika JP. Ferroelectricity in the Ilmenite Structure. Phys Rev 1949;76:1886–7. https://doi.org/10.1103/PhysRev.76.1886.2.
[2] Weis RS, Gaylord TK. Lithium niobate: Summary of physical properties and crystal structure. Appl Phys A 1985;37(4):191–203. https://doi.org/10.1007/BF00614817.
[3] Boyd GD, Miller RC, Nassau K, Bond WL, Savage A. $LiNbO_3$: An efficient phase matchable nonlinear optical material. Appl Phys Lett 1964;5:234–6. https://doi.org/10.1063/1.1723604.
[4] Ballman AA. Growth of piezoelectric and ferroelectric materials by the Czochralski technique. J Am Ceram Soc 1965;48:112–3. https://doi.org/10.1111/j.1151-2916.1965.tb11814.x.
[5] Savage A. Pyroelectricity and spontaneous polarization in $LiNbO_3$. J Appl Phys 1966;37:3071–2. https://doi.org/10.1063/1.1703164.
[6] Dixon RW. Photoelastic properties of selected materials and their relevance for applications to acoustic light modulators and scanners. J Appl Phys 1967;38:5149–53. https://doi.org/10.1063/1.1709293.
[7] Chen FS. Optically induced change of refractive indices in $LiNbO_3$ and $LiTaO_3$. J Appl Phys 1969;40:3389–96. https://doi.org/10.1063/1.1658195.
[8] Glass AM, von der Linde D, Negran TJ. High-voltage bulk photovoltaic effect and the photorefractive process in $LiNbO_3$. Appl Phys Lett 1974;25:233–5. https://doi.org/10.1063/1.1655453.
[9] Graham RA. Pressure dependence of the piezoelectric polarization of $LiNbO_3$ and $LiTaO_3$. Ferroelectrics 1976;10:65–9. https://doi.org/10.1080/00150197608241952.
[10] Kaminow IP, Turner EH, Barns RL, Bernstein JL. Crystallographic and electrooptic properties of cleaved $LiNbO_3$. J Appl Phys 1980;51:4379–84. https://doi.org/10.1063/1.328301.
[11] Arizmendi L. Photonic applications of lithium niobate crystals. Phys Status Solid (a) 2004;201:253–83. https://doi.org/10.1002/pssa.200303911.
[12] Sohler W, Hu H, Ricken R, Quiring V, Vannahme C, Herrmann H, et al. Integrated optical devices in lithium niobate. Opt Photonics News 2008;19:24–31. https://doi.org/10.1364/OPN.19.1.000024.
[13] Y. Yao, B. Liu, H. Zhang, H. Liu, and J. Liu, "Design of thin-film lithium niobate structure for integrated filtering and sensing applications." Res. Phys. 17 (2020) 103082-11pp. https://doi.org/10.1016/j.rinp.2020.103082.
[14] Courjal N, Bernal M-P, Caspar A, Ulliac G, Bassignot F, Gauthier-Manuel L, et al. "Lithium niobate optical waveguides and microwaveguides," in *Emerging Waveguide Technology* (London, UK. In: You KY, editor. Emerging Waveguide Technology. InTech; 2018.
[15] Wooten EL, Kissa KM, Yi-Yan A, Murphy EJ, Lafaw DA, Hallemeier PF, et al. A review of lithium niobate modulators for fiber-optic communications systems. IEEE J Sel Top Quantum Electron 2000;6:69–82. https://doi.org/10.1109/2944.826874.
[16] Chen JY, Ma ZH, Sua YM, Li Z, Tang C, Huang YP. Ultra-efficient frequency conversion in quasi-phase-matched lithium niobate microrings. Optica 2019;6:1244–5. https://doi.org/10.1364/OPTICA.6.001244.
[17] Myers LE, Bosenberg WR. Periodically poled lithium niobate and quasi-phase-matched optical parametric oscillators. IEEE J Quantum Electron 1997;33:1663–72. https://doi.org/10.1109/3.631262.
[18] C. Zhao, W. Geng, X. Qiao, F. Xue, J. He, G. Xue, Y. Liu, H. Wei, K. Bi, Y. Li, M. Xun, X. Chou, "Anti-irradiation SAW temperature sensor based on 128° YX $LiNbO_3$ single crystal." Sens. & Act. A: Phys. 333 (2022) 113230-8pp. .
[19] M. Yu, Y. Okawachi, R. Cheng, C. Wang, M. Zhang, A. L. Gaeta, and M. Loncar, "Raman lasing and soliton mode-locking in lithium niobate microresonators." Light: Sci. & Appl. 9 (2020) 9-7pp. https://doi.org/10.1038/s41377-020-0246-7.
[20] Iyi N, Kitamura K, Izumi F, Yamamoto JK, Hayashi T, Asano H, et al. Comparative study of defect structures in lithium niobate with different compositions. J Sol St Chem 1992;101:340–52. https://doi.org/10.1016/0022-4596(92)90189-3.
[21] Rahman MKR, Riscob B, Bhatt R, Bhaumik I, Ganesamoorthy S, Vijayan N, et al. Investigations on crystalline perfection, Raman spectra and optical characteristics of transition metal (Ru) co-doped Mg:$LiNbO_3$ single crystals. ACS Omega 2021;6:10807–15. https://doi.org/10.1021/acsomega.1c00452.
[22] Scott J, Mailis S, Sones CL, Eason RW. A Raman study of single-crystal congruent lithium niobate following electric-field repoling. Appl Phys A 2004;79:691–6. https://doi.org/10.1007/s00339-003-2249-7.
[23] M. D. Fontana and P. Bourson, "Microstructure and defects probed by Raman spectroscopy in lithium niobate crystals and devices." Appl. Phys. Rev. 2 (2015) 040602-14pp. https://doi.org/10.1063/1.4934203.
[24] https://www.mtixtl.com/linbo3opticalgradez-cut10x102sp.aspx (Accessed March 2023).
[25] Schlarb U, Klauer S, Wesselmann M, Betzler K, Wiihlecke M. Determination of the Li / Nb ratio in lithium niobate by means of birefringence and Raman measurements. Appl Phys A 1993;56:311–5. https://doi.org/10.1007/BF00324348.
[26] Kovács L, Ruschhaupt G, Polgár K, Corradi G, Wohlecke M. Composition dependence of the ultraviolet absorption edge in lithium niobate. Appl Phys Lett 1997;70:2801–3. https://doi.org/10.1063/1.119056.
[27] A. R. Zanatta, "The optical bandgap of lithium niobate ($LiNbO_3$) and its dependence with temperature." Res. Phys. 39 (2022) 105736-3pp. https://doi.org/10.1016/j.rinp.2022.105736.
[28] Menendez J, Cardona M. Temperature dependence of the first-order Raman scattering by phonons in Si, Ge, and α-Sn: Anharmonic effects. Phys Rev B 1984;29:2051–9. https://doi.org/10.1103/PhysRevB.29.2051.
[29] See, for example, A. R. Zanatta, "Temperature-dependent Raman scattering of the Ge + GeO_x system and its potential as an optical thermometer." Res. Phys. 19 (2020) 103500-9pp, and references therein. https://doi.org/10.1016/j.rinp.2020.103500.
[30] Mendes-Filho J, Lemos V, Cerdeira F. Pressure dependence of the Raman spectra of $LiNbO_3$ and $LiTaO_3$. J Raman Spec 1984;15:367–9. https://doi.org/10.1002/jrs.1250150602.
[31] Yao SH, Wang JY, Liu H, Yan T, Yu DH, Chen YF. Mechanism of the abnormal thermal expansion of nearly stoichiometric $LiNbO_3$. J Crystal Growth 2011;318:951–3. https://doi.org/10.1016/j.jcrysgro.2010.10.052.
[32] Sidorov NV, Kruk AA, Yanichev AA, Palatnikov MN, Kalinnikov VT. Manifestation of birefringence in lithium niobate crystal in photorefractive and Raman scattering. Dokl Phys Chem 2014;459:173–6. https://doi.org/10.1134/S0012501614110025.
[33] Kruk AA, Sidorov NV, Yanichev AA, Palatnikov MN. Raman spectra of copper-doped lithium niobate crystals as a function of excitation wavelength. J Appl Spectrosc 2014;81:1–6. https://doi.org/10.1007/s10812-014-9878-9.

[34] Paz-Pujalt GR, Tuschel DD. Depth profiling of proton exchanged $LiNbO_3$ waveguides by micro-Raman spectroscopy. Appl Phys Lett 1993;62:3411–3. https://doi.org/10.1063/1.109033.
[35] Huang HC, Dadap JI, Gaathon O, Herman IP, Osgood RM, Bakhru S, et al. A micro-Raman spectroscopic investigation of He^+-irradiation damage in $LiNbO_3$. Opt Mater Express 2013;3:126–42. https://doi.org/10.1364/OME.3.000126.
[36] Dawson P. Polarization measurements in Raman spectroscopy. Spectrochim Acta 1972;28A:715–23. https://doi.org/10.1016/0584-8539(72)80040-0.
[37] S. Sanna and W. G. Schmidt, "$LiNbO_3$ surfaces from a microscopic perspective." J. Phys.: Condens. Matter 29 (2017) 413001-48pp. https://doi.org/10.1088/1361-648X/aa818d.